Philosophical Magazine,
Vol. 00, No. 00, DD Month 200x, 1–10

Electron-phonon interaction and superconductivity in the borocarbide superconductor $ScNi_2B_2C$

H. M. Tütüncü*[1,2], Ertuğrul Karaca[1,2], G. P. Srivastava[3]

[1]Sakarya Üniversitesi, Fen-Edebiyat Fakültesi, Fizik Bölümü, 54187, Adapazarı, Turkey

[2]Sakarya Üniversitesi, Biyomedikal, Manyetik ve Yarıiletken Malzemeler Araştırma Merkezi (BIMAYAM), 54187, Adapazarı, Turkey

[3]School of Physics, University of Exeter, Stocker Road, Exeter EX4 4QL, UK

(Received 00 Month 200x; in final form 00 Month 200x)

We have made an *ab initio* investigation of electron-phonon interaction and superconductivity in the borocarbide superconductor $ScNi_2B_2C$ adopting the body-centered tetragonal $LuNi_2B_2C$-type of layered crystal structure. The calculated electronic structure and density of states suggest that the bonding is a combination of covalent, ionic and metallic in nature and that the Fermi level falls in one of the peaks in the electronic density of states. Our electron-phonon interaction calculations suggest that the mechanism for superconductivity is heavily governed by interactions of electrons with acoustic phonon modes and low-frequency optical phonon modes, which strongly modulate NiB_4 tetrahedral bond angles. By integrating the Eliashberg spectral function, the value of average electron-phonon coupling parameter is found to be 0.93 and the superconducting critical temperature is calculated to be 16.28 K, in excellent agreement with the experimentally reported value of 16.0 K.

1 Introduction

The nickel borocarbides RNi_2B_2C (R = Y, Lu, Sc, Tm, Er, Ho, and Dy) have received much interest due to their interesting physical properties [1–30]. Many of these compounds exhibit superconductivity with superconducting temperatures (T_c) as high as 16.5, 15.6 and 16.0 found for the Lu [12], Y [12] and Sc [15] compounds, respectively. Some of these borocarbides ($HoNi_2B_2C$, $ErNi_2B_2C$, $TmNi_2B_2C$, $DyNi_2B_2C$) [4, 5, 8–10, 20, 22–24, 28, 30] exhibit, however, antiferromagnetic ordering with the Néel temperature (T_N) comparable to T_c. Due to the wide range of T_N, together with relatively high values of T_c, there are better chances of finding the interplay between magnetism and superconductivity in these systems. Their structure basically contains NiB_4 tetrahedra between layers of RC with a rocksalt structure and where the Ni-B bond generates a corrugated plane. To clarify the superconducting properties of YNi_2B_2C and $LuNi_2B_2C$, countless band structure calculations [31–43] have been performed for these borocarbides. Although their structure resembles that of the cuprate high-temperature superconductors, theoretical band structure calculations for YNi_2B_2C and $LuNi_2B_2C$ foresee a three-dimensional electronic structure with considerable contributions from all atoms to the metallic character of these compounds [31–43]. A characteristic feature of the borocarbide superconductors is the existence of a flat band near the Fermi level, which causes a peak in the electronic density of states and thus leads to an enhancement of the superconducting correlations present in these materials [31–43]. For example, in the compound $LuNi_2B_2C$ [43], the corresponding flat band, which is Ni-d derived, coincides with the Fermi level along the Γ-X ([110]) symmetry direction of the Brillouin zone. Furthermore, Mattheiss, Siegrist, and Cava [32] conclude that superconductivity in YNi_2B_2C and $LuNi_2B_2C$ can be related to a conventional electron-phonon mechanism that couples the sp-like conduction electrons to a high-frequency boron A_{1g} phonon mode in which the boron atoms vibrate along the z axis relative to the remaining atoms. However, detailed information on phonon spectrum is a prerequisite for making a more persuasive conclusion. Thus, in 2005 a density functional perturbation

* Corresponding author. Email: tutuncu@sakarya.edu.tr

Philosophical Magazine
ISSN 1478-6435 print/ISSN 1478-6443 online
http://www.tandf.co.uk/journals
DOI: 10.1080/1478643YYxxxxxxxx

approach was used by Reichardt *et al* [44] for investigating phononic and electron-phonon interaction properties of YNi_2B_2C. The prediction of Mattheis and co-workers [32] of involving the zone-center A_{1g} mode is affirmed by the work of Reichardt *et al* [44]. However, they mention that the coupling of this phonon mode with electrons diminishes rapidly with increasing wave vector [44]. Furthermore, they find that the contribution of the A_{1g} mode to the average electron-phonon coupling parameter (λ) is only 4% [44]. On the other hand, about 70% of λ comes from the nine lowest branches [44]. This implies that low-frequency optical phonon modes and acoustic phonon modes are more involved in the process of scattering of electrons than high frequency optical phonon modes, which result from the vibrations of B and C atoms. Recently, we have presented first-principles calculations of the band structure, the phonons and the electron–phonon interaction in superconducting $LuNi_2B_2C$ (T_c around 16 K) within the framework of the the generalized gradient approximation of density functiona theory [43]. This recent work [43] also shows that the strong coupling of the high-frequency boron A_{1g} phonon mode to the s-p band near the Fermi level mentioned by previous theoretical calculations [32, 33] does not seem to be essential either, though it makes some contribution to the superconductivity in $LuNi_2B_2C$, since the contributions from B and C to the density of states at the Fermi level $N(E_F)$ are much smaller than that from Ni. In other words, a large $N(E_F)$ is contributed mainly from Ni atoms and the partially strong electron-phonon coupling together account for T_c around 16 K [43].

Although considerable progress has been made towards experimental measurement and description of superconductivity in the nickel borocarbide $ScNi_2B_2C$ [3, 7, 12, 15, 19], to the best of our knowledge no experimental or theoretical work has been performed for the electronic, lattice dynamic and electron-phonon interaction properties of this superconductor. Our previous work [43] shows that the density functional theory [45] provides a trustworthy framework for implementing from first principles the Migdal-Eliashberg approach for calculating the superconducting properties of borocarbide superconductors. Thus, in the light of our previous work [43], we have studied the structural and electronic properties of $ScNi_2B_2C$ and compared them with the results for $LuNi_2B_2C$ [43]. As expected, a qualitatively similar electronic structure is found with appreciable contributions from all sites. A density functional linear response approach has then been used for a detailed investigation of lattice dynamics and electron–phonon interaction properties of $ScNi_2B_2C$. Our electron-phonon interaction calculations reveal that $ScNi_2B_2C$ is a conventional with medium electron phonon coupling parameter of 0.93 in which the relatively high T_c of 16.28 K arises from a large value of the density of states at the Fermi level.

2 Theory

Our calculations have been performed using the Quantum-Espresso (QE) package [45] which is based on the density functional theory (DFT) for total energy calculations. Ultrasoft pseudopotentials [46, 47] are used to simulate interactions of valence electrons with ion cores, and the electron wave function is expanded in plane waves up to an energy cutoff of 60 Ry for all calculations. The exchange–correlation energy is evaluated using the generalized gradient approximation (GGA) of the Perdew–Burke–Ernzerhof (PBE) formalism [48], which is dependent on both the electron density and its gradient at each space point. The Kohn-Sham equations [49] are solved using an iterative conjugate gradient scheme, employing a set of Monkhorst-Pack special $\boldsymbol{k}$ points [50]. Integration over the Brillouin zone (BZ) for total-energy calculations has been performed using the 8×8×8 zone-centred grid, producing 59 $\boldsymbol{k}$ points in the irreducible part of the BZ (IBZ). The self-consistent electronic structure calculations are carried out by using the 24×24×24 zone-centred grid, producing 1063 $\boldsymbol{k}$ points in the IBZ.

The phonon spectrum and electron-phonon coupling functions are calculated using the linear response method within the generalized gradient approximation [43, 45, 51]. The Brillouin zone integrations for charge self-consistency during linear response phonon calculations are carried out using a 8×8×8 grid of $\boldsymbol{k}$ points. The calculation of dynamical matrices for $ScNi_2B_2C$ are carried out using a 4×4×4 grid resulting in 13 irreducible $\boldsymbol{q}$ points. Then, these dynamical matrices are Fourier transformed to calculate phonons for any chosen $\boldsymbol{k}$ point. The phonon density of states and the electron-phonon matrix elements are then used to obtain the Eliashberg spectral function from which the superconducting properties of the materials are achieved. Fermi-surface sampling for the evaluation of the electron-phonon matrix elements has been

performed by using 24×24×24 $\boldsymbol{k}$-mesh with a Gaussian width 0.01 Ry. The phonon density of states and the Eliashberg function are also calculated by using this $\boldsymbol{k}$-mesh.

3 Results

3.1 *Structural and Electronic Properties*

$ScNi_2B_2C$ crystallizes in the body centered tetragonal $LuNi_2B_2C$-like layered structure with space group I4/mmm. Its primitive unit cell includes one formula unit (six atoms), and the atoms occupy the Wyckoff positions 2(a) [(0,0,0)] for Sc, 4(d) [(0, 1/2, 1/4), (1/2, 0, 1/4)] for Ni, 4(e) [(0, 0, z), (0, 0,-z)] for B and (2b) [(0, 0, 1/2)] for C, where z is the internal free coordinate. Thus, this structure is defined by two lattice parameters, a and c, and one internal structural parameter, z. To start with, the structural optimization of $ScNi_2B_2C$ has been carried out using the total energy minimization and zero atomic force criteria. The values of bulk modulus (B) and its pressure derivative ($B^{'}$) have been found by minimizing the crystal total energy for different values of crystal volume and using the Murnaghan equation of state [52]. Our results of the calculated lattice constants (a and c), bulk modulus (B), its pressure derivative ($B^{'}$), and the optimized internal parameter (z) are presented Tab. 1. As can be seen from this table, available experimental results for the lattice parameters (a and c) are not very consistent with each other. However, our theoretical results for a and c differ from the latest experimental values [19] of 3.35 $\mathring{A}$ and 10.68 $\mathring{A}$ by 1.2% and 0.6%, respectively. To the best of our knowledge, experimental data are not available for bulk modulus and its pressure derivative.

Fig. 1(a) shows the atomic arrangement in the tetragonal unit cell of $ScNi_2B_2C$, and selected bond-lengths and bond angles are presented in Tab. 1. This structure consists of tetrahedrally bonded, square Ni_2B_2 layers, separated by square rocksalt like ScC. Very strong boron-carbon bonds join the two layers. In this structure, each nickel atom coordinates with four boron atoms, generating a distorted tetrahedra with two different angles (α and β in Fig. 1(a)). The coordination sphere of nickel atom is completed by four neighboring nickel atoms with the interatomic distance of 2.398 $\mathring{A}$. This can be considered a strong Ni-Ni metallic bond because the Ni-Ni distance in $ScNi_2B_2C$ is considerable shorter than the corresponding distance value of 2.49 $\mathring{A}$ in the fcc nickel structure. The Ni-B distance is found to be 2.063 $\mathring{A}$ which is slightly shorter than the sum of the covalent radii for Ni and B of 2.08 $\mathring{A}$. Each boron has five–fold pyramidal coordination with four nickel atoms and one apical carbon atom. The shortest interatomic distance in the structure occurs for B-C (1.481 $\mathring{A}$), considerably shorter than the sum of the covalent radii for B and C of 1.54 $\mathring{A}$. Thus, we can conclude that the B and C atoms are bonded not only by ionic interaction, but also covalently. The same conclusion can be made for the Ni and B atoms. As a consequence, the bonding in the $ScNi_2B_2C$ structure is primarily of covalent-ionic nature with the existence of some metallic character.

The Brillouin zone of body-centered tetragonal lattice is shown in Fig. 1(b). Fig. 2 (a) presents the calculated energy band structure of $ScNi_2B_2C$ along several high-symmetry directions which are shown in Fig. 1(b). For the sake of comparison, the electronic structure of $LuNi_2B_2C$ is also shown in Fig. 2 (b). The electronic structures of both materials look similar to each other. This result is totally expected because these materials are isostructural as well as isoelectronic to each other. In our previous work [43], we have discussed the electronic structure of $LuNi_2B_2C$ in detail and thus we will only discuss the electronic structure of $ScNi_2B_2C$ in this work. Several bands cross the Fermi level, rendering clear metallic nature of the system. Due to the strong covalent interaction between constituents, the dispersion bands along the [001] direction (Γ-Z) is analogous to that in the plane (Γ-X), indicating three-dimensional character of the band structure. In order to analysis the nature of the electronic structure in detail, the total and the angular momentum decomposition of the atom projected density of states (DOS) for $ScNi_2B_2C$ are calculated. Fig. 3 illustrates the total, and s, p, and d projected DOS at the Sc, Ni, B and C atomic sites. The lowest band in the energy region from -14.0 to -12.7 eV consists of C 2s states and is separated by a gap of 1.9 eV from the higher valence band region. The orbital character of the higher valence band region complex, which starts at around -10.8 eV, changes gradually from B 2s to B 2p-C 2p and finally to Ni 3d states near the Fermi level. We can see that the DOS features below -8.2 eV are mainly contributed by B and C electronic states. Furthermore, B s and C p exhibit strong hybridization with each other in

the range -10.8 to -8.2 eV, revealing strong B-C covalent bonding. The energy range from -8.2 to -4 eV is predominated by the Ni, B and C atoms with only a weak mixture of Sc atoms. In the energy window from -4 to -1 eV, the DOS peaks arise from Ni-3d like bands with low $E(k)$ dispersion in this energy region. These states participate in metallic like Ni-Ni interaction. A notable feature in the electronic structure is the presence of almost flat bands along the Γ-X and Γ-P symmetry lines, which give rise to a peak in the DOS very close to the Fermi level. This peak is mainly dominated by Ni atoms with appreciable contributions from all other constituents Sc, B, and C as well. The Fermi level occurs near the top of this peak. This may be one of the reasons for this material to become superconductor since Cooper pairs in the BCS theory are produced by electrons which have energies close to the Fermi energy. A similar observation has been made for $LuNi_2B_2C$. As a consequence, we can conclude that the band structures of $ScNi_2B_2C$ and $LuNi_2B_2C$ are very similar to each other. Our electronic calculations produce the value of density of states at the Fermi level ($N(E_F)$) to be 3.33 States/eV which is comparable to the corresponding value of 3.64 States/eV for $LuNi_2B_2C$ [43]. The contributions of Sc, Ni, B and C elements to $N(E_F)$ are about 20%, 61%, 15% and 4%, respectively. In particular, the orbital characters at E_F consist of Ni d, Sc d, B p, Ni p and C p. The contributions of these electronic states to $N(E_F)$ are about 46%, 19%, 13%, 13% and 3%, respectively. Although $N(E_F)$ is mainly dominated by Ni atoms, all four atoms are involved in the formation of bands just below and above the Fermi level. In particular, the second largest contribution to $N(E_F)$ comes from Sc d states because Sc is not fully ionized to the 3+ state. Hence, it is expected that electrons responsible for the superconductivity are mainly of d character of Ni and Sc atoms. Finally, the calculated Fermi surface of $ScNi_2B_2C$ is illustrated in Fig. 4. As noted in Fig. 3, the characters of the Fermi surface are primarily constituted by Ni 3d, Sc 3d, Ni 4d, and B and C 2p states. The features of this complex Fermi surface are similar to those of $LuNi_2B_2C$ [53].

3.2 *Phonons and electron-phonon interaction*

The zone-centre phonon modes for $ScNi_2B_2C$ can be categorized by the irreducible representation of the point group D_{4h} (4/mmm). As obtained from the group theory, the symmetries of the optical zone-centre phonon modes are:

$$\Gamma(D_{4h}) = 3E_u + 3A_{2u} + B_{1g} + 2E_g + A_{1g},$$

with A, B and E modes being singly, singly and doubly degenerate, respectively. The frequencies of these zone-centre phonon modes are given together with their electron-phonon coupling parameters (λ) in Tab. 2. As can be seen from this table, the electron-phonon coupling parameters of the B_{1g} and A_{1g} phonon modes are considerably larger than the corresponding values for the remaining phonon modes. The eigenvector representations, displayed in Fig. 5, clearly suggest these phonon modes dynamically modify the tehrahedral bond angles in NiB_4 and consequently make large contribution to the electron-phonon coupling parameter. We note that the A_{1g} phonon mode contains vertical B vibrations which can stretch/compress the linear B-C-B bonds. However, we can not say that these phonon modes are crucial for superconductivity in $ScNi_2B_2C$ because their electron-phonon coupling parameters are too low to produce the superconducting transition temperature around 16 K. Furthermore, the electron-phonon coupling parameters of these phonon modes diminish considerably with increased $\boldsymbol{q}$ wave vector, as can be seen from Fig. 6.

For a realistic discussion of electron-phonon coupling parameter λ it is important to examine the electron-phonon matrix element involving phonons of all polarizations throughout the Brillouin zone. We present the results for the phonon dispersion relations for $ScNi_2B_2C$ in Fig. 7(a) along several symmetry directions. For the sake of comparison, the phonon dispersion curves of $LuNi_2B_2C$ are also shown in Fig. 7(b). As we have observed for their electronic band structures, the phonon band structures of $ScNi_2B_2C$ and $LuNi_2B_2C$ [43] are similar to each other. As can be seen from Fig. 7(a), the total phonon spectrum of $ScNi_2B_2C$ with eighteen branches splits into four apparent regions. The three acoustic and six optical branches extend up to 10.5 THz in the first frequency region. The acoustic phonon branches disperse up to 7.0 THz and there is considerable degree of overlap between the acoustic and low-lying optical phonon modes in this frequency region. The second frequency region from 11.2 to 14.8 THz contains seven optical branches

which are also dispersive like the optical phonon modes in the first frequency region. These two regions are separated from each other by a gap of 0.7 THz. The third region from 25.8 to 27.0 THz includes only one optical phonon branch which is separated by a large gap of 11 THz from the seven optical phonon modes distributed in the second region. The fourth region also contains only one optical phonon mode extending from 39.8 to 40.4 THz. A large gap region of 12.8 THz separates the last two regions from each other. The nature of the phonon spectrum can be understood much better by the total and partial phonon density of states (see Fig. 8). Modes in the first phonon band region involve displacements of all four atomic species. We remark that the contribution of Ni atoms is strongest between 4.8 and 5.9 THz and almost vanishes above the first phonon band region. Thus, Ni atoms contribute to acoustic phonon branches and low-lying optical phonon branches. Large overlap between B and C vibrations exist between 10.5 and 14.8 THz due to the strong covalent bonding between these atoms. The sharp peak at around 26.3 THz is formed by the vibrations of B atoms while the strong peak at around 39.9 THz arises from the coupled motion of B and C atoms.

The most remarkable feature in the phonon spectrum of $ScNi_2B_2C$ is the anomalous dispersion relations of the first transverse acoustic branch (TA_1) and the A_{2u} branch (see Fig. 7(a)). In order to examine the effect of these softenings on electron-phonon interaction in $ScNi_2B_2C$, we have plotted the mode-dependent electron-phonon coupling parameter $\lambda_{\mathbf{q},j}$ of these phonon modes in Fig. 9(a). This figure reveals that the anomalous dispersion of these phonons produces large electron-phonon coupling parameters. We have to mention that a similar observation has been mode for the electron-phonon interaction in $LuNi_2B_2C$, YPd_2B_2C and YPt_2B_2C in our previous *ab initio* work [43]. The electron-phonon coupling parameter of TA_1 branch reaches its largest value of 1.19 at $\boldsymbol{q} = \frac{2\pi}{a}$ (0.5, 0.0, 0.0) which is much larger than the electron-phonon coupling parameter of the zone-center A_{1g} phonon mode (see Fig. 9(a)). Now, it will be rewarding to analyze the eigenvector representation of the TA_1 phonon mode at at $\boldsymbol{q} = \frac{2\pi}{a}$ (0.5, 0.0, 0.0) which is shown in Fig. 9(b). As can be seen from this figure, this phonon mode is created by the coupled motion of Ni, B and C atoms. Thus, the atomic displacement pattern of this phonon mode strongly modulates the NiB_4 bond angles which gives rise to significantly large electron-phonon coupling parameter for this phonon mode.

To find the strengths with which the different modes of atomic vibration couple to electrons, and thus are skillful in effectuating the superconducting properties most, we illustrate the Eliashberg spectral function $\alpha^2F(\omega)$ in Fig. 10. From the integration of the Eliashberg spectral function one can obtain the average electron-phonon coupling constant λ, which represents a good measure of the overall strength of the electron-phonon interaction: it is given by

$$\lambda = 2 \int \frac{\alpha^2 F(\omega)}{\omega} d\omega. \tag{1}$$

From the above equation, the value of λ is determined to be 0.93 which obviously shows that the electron-phonon interaction in this material is of medium strength. This value is comparable to the electron-phonon coupling parameter of 0.83 for $LuNi_2B_2C$ [43]. A critical assessment of the Eliashberg spectral function reveals the importance of acoustic and low-frequency optical phonon modes in the lowest phonon band. It is worth to mention that the value of the electron-phonon coupling parameter increases rapidly with rising frequency in this frequency range. The phonon modes in this region contribute about 77% (0.72) to λ. The second largest contribution to λ within around 20% comes from the phonon modes between 11.2 and 14.8 THz. This contribution is acceptable because the coupled B-C atomic vibrations are dominant in this frequency region and B and C orbitals make much lesser contributions to $N(E_F)$ compared to the contribution of Ni orbitals. The contributions of A_{1g} and A_{2u} phonon modes to λ are around 2% and 1%, respectively. From the analysis presented above, we can conclude that the three acoustic phonon branches and low-frequency optical phonon branches are more involved in the process of scattering of electrons than high-frequency optical phonon modes.

Finally, the value of the superconducting transition temperature T_c can be calculated from the Allan-

Dynes modification of the McMillian formula [54]

$$T_c = \frac{\omega_{\ln}}{1.2}\exp\left(-\frac{1.04(1+\lambda)}{\lambda-\mu^*(1+0.62\lambda)}\right), \tag{2}$$

which connects T_c with λ, the logaritically averaged phonon frequency $\omega_{\ln} = \exp\left(2\lambda^{-1}\int_0^\infty \frac{\mathrm{d}\omega}{\omega}\alpha^2F(\omega)\ln\omega\right)$, and the effective screened Coulomb repulsion constant μ^*. The value of μ^* is taken to be 0.10 while the value of $\omega_{\ln}$ is computed to be 263.58 K. Putting the values of λ, $\omega_{\ln}$ and μ^* into the Allan-Dynes modification of the McMillian formula, the value of T_c is obtained to be 16.28 K, which is surprisingly is very close the experimentally measured value of around 16.0 K [15]. Furthermore, the electron–phonon coupling constant λ also enters the electronic specific heat coefficient γ, which is given as

$$\gamma = \frac{1}{3}\pi^2 k_B^2 N(E_F)(1+\lambda). \tag{3}$$

Using this equation, the value of γ for $ScNi_2B_2C$ is calculated to be 15.1 $mJmol^{-1}K^{-2}$ which compares very well with the calculated γ value of 15.7 $mJmol^{-1}K^{-2}$ for $LuNi_2B_2C$. However, no experimental data is available for comparison. We, thus emphasize that in spite of its layered structure, superconductivity in $ScNi_2B_2C$ can be explained in terms of the conventional BCS strong-coupling theory, similar to $LuNi_2B_2C$ [43].

From the several remarks made above about the similarity of some results between $ScNi_2B_2C$ and its isostructural compound $LuNi_2B_2C$, it would indeed be useful to make a comparison between their superconducting properties by examining their electronic and phonon structures. A comparison of their superconducting parameters has been presented in Tab. 3. It is well known that there are three main factors which influence T_c for the BCS-type superconductors. These factors are the electronic DOS at the Fermi level ($N(E_F)$), the logarithmic average phonon frequency (ω_{ln}), and the strength of electron-phonon coupling parameter (λ). As regards the electronic structure, the value of $N(E_F)$ decreases from 3.64 States/eV to 3.33 States/eV when our material is changed from $LuNi_2B_2C$ to $ScNi_2B_2C$. This change modulates the value of λ because it is directly related to the change in $N(E_F)$ according to the McMillan-Hopfield expression $\lambda = \frac{N(E_F)<I^2>}{M<\omega^2>}$, where $< I^2 >$ is the averaged square of the electron-phonon matrix, $< \omega^2 >$ is the averaged square of the phonon frequency, and M is the mass involved. However, λ of $ScNi_2B_2C$ is slightly larger than that of $LuNi_2B_2C$. In order to explain this difference, we should examine the lattice dynamical properties of these materials. The value of ω_{ln} for $ScNi_2B_2C$ is smaller than that for $LuNi_2B_2C$. Although softer phonon frequencies give rise to smaller ω_{ln} (see Tab. 3), they make a positive contribution to the electron-phonon coupling parameter due to the McMillan-Hopfield expression. Thus, the smaller value of ω_{ln} for $ScNi_2B_2C$ makes its λ larger than that of $LuNi_2B_2C$. As a consequence, the value of T_c for $ScNi_2B_2C$ is slightly larger than that for $LuNi_2B_2C$.

4 Summary

In this work, we examined the structural, electronic, lattice dynamical and electron-phonon interaction properties of $ScNi_2B_2C$ adopting the body-centered tetragonal $LuNi_2B_2C$ structure by using the generalized gradient approximation of the density functional theory and the plane wave *ab initio* pseudopotential method. Our results suggest a three dimensional electronic structure for this compound with significant contributions from all of the constituent atoms to its metallic character, although the largest contribution to $N(E_F)$ comes from Ni atoms. The Fermi level falls on the peak of its electronic density, providing the first reason for this material to become superconductor. The most interesting features in the phonon spectrum of this material are the phonon anomalies of TA_1 and A_{2u} branches along the Γ-G1-Z symmetry direction. We have shown that these phonon anomalies make large contribution to the average electron-phonon coupling parameter of $ScNi_2B_2C$. Thus, we believe that this is the second reason for this material to become superconductor. Our calculations reveal that the electronic and phonon band structures of

$ScNi_2B_2C$ and $LuNi_2B_2C$ are similar to each other in several respects and thus these borocarbides have very similar superconducting properties.

A critical assessment of the Eliashberg spectral function suggests that acoustic and low-frequency optical branches more involved in the progress of scattering of electrons rather than high-frequency optical phonon modes. More particularly, our electron-phonon interaction calculations suggest a conventional electron-phonon mechanism for superconductivity in $ScNi_2B_2C$ involving acoustic and low-frequency optical phonon modes that dynamically modulate the NiB_4 tetrahedra angles. The average electron-phonon coupling parameter is calculated to be 0.93, suggesting that $ScNi_2B_2C$ is a phonon-mediated superconductor with medium electron-phonon coupling strength. Using the Allen-Dynes modified McMillian equation with the screened Coulomb pseudopotential parameter $\mu^* = 0.10$, the superconducting temperature is estimated to be 16.28 K which compares very well with the experimentally reported value of 16.0 K.

ACKNOWLEDGEMENTS

Some of the calculations for this project were carried out using the computing facilities on the Intel Nehalem (i7) cluster (ceres) in the School of Physics, University of Exeter, United Kingdom.

References

[1] R. J. Cava, H. Takagi, H. W. Zandbergen, J. J. Krajewski, W. F. Peck Jr., T. Siegrist, B. Batlogg, R. B. van Dover, R. J. Felder, K. Mizuhashi, J. O. Lee, H. Eisaki, S. Uchida, Superconductivity in the quaternary intermetallic compounds $LnNi_2B_2C$, Nature 367 (1994), pp.252–253.

[2] S. A. Carter, B. Batlogg, R. J. Cava, J. J. Krajewski, W. F. Peck, and H. Takagi, Electron density of states in the borocarbide intermetallic snyercondnctors, Phys. Rev. B 50 (1994), pp. 4216–4219.

[3] H. C. Ku, C. C. Lai, Y. B. You, J. H. Shieh and W. Y. Guan, Superconductivity at 15 K in the metastable $ScNi_2B_2C$ compound, Phys. Rev. B 50 (1994), pp. 351–353.

[4] T. E. Grigereit, J. W. Lynn, Q. Huang, A. Santoro, R. J. Cava, J. J. Krajewski, and W. F. Peck, Jr., Observation of Oscillatory Magnetic Order in the Antiferromagnetic Superconductor $HoNi_2B_2C$, Phys. Rev. Lett. 73 (1994), pp. 2756–2759.

[5] M. S. Lin, J. H. Shieh, Y. B. You, W. Y. Guan, H. C. Ku, H. D. Yang, and J. C. Ho, Magnetic transitions and nearly reentrant superconducting properties $HoNi_2B_2C$, Phys. Rev. B 52 (1995), pp.1181–1186.

[6] H. Michor, T. Holubar, C. Dusek, and G. Hilscher, Specific-heat analysis of rare-earth transition-metal borocarbides: An estimation of the electron-phonon coupling strength, Phys. Rev. B 52 (1995), pp. 16165–16175.

[7] C. C. Lai, M. S. Lin, Y. B. You, and H. C. Ku, Systematic variation of superconductivity for the quaternary borocarbide system RNi_2B_2 (R = Sc, Y, La, Th, U, or a lanthanide), Phys. Rev. B 51 (1995), pp. 420–423.

[8] Q. Huang, A. Santoro, T. E. Grigereit, J. W. Lynn, R. J. Cava, J. J. Krajewski, and W. F. Peck, Jr., Neutron-powder-diffraction study of the nuclear and magnetic structures of the antiferromagnetic superconductor $HoNi_2B_2C$, Phys. Rev. B 51 (1995), pp. 3701–3708.

[9] B. K. Cho, P. C. Canfield, and D. C. Johnston, Onset of superconductivity in the antiferromagnetically ordered state of single-crystal $DyNi_2B_2C$, Phys. Rev. B 52 (1995), pp. 3844–3847(R).

[10] H. Schmidt and H. F. Braun, Superconductivity, magnetism, and their coexistence in $R(Ni_{1-x}\ Co_x)_2B_2$ C (R= Lu, Tm, Er, Ho, Dy), Phys. Rev. B 55 (1997), pp. 8497–8505.

[11] In-Sang Yang, M. V. Klein, S. L. Cooper, P. C. Canfield, B. K. Cho, and Sung-Ik Lee, Study of the superconducting gap in RNi_2B_2C (R = Y, Lu) single crystals by inelastic light scattering, Phys. Rev. B 62 (2000), pp. 1291–1295.

[12] K.H. Muller and Vladimir Narozhnyi (Eds.), Proceedings of the NATO Advanced Research Workshop on Rare Earth Tansition Metal borocarbides (Nitrides): Superconducting, Magnetic and Normal State Properties, Dresden, Germany, June 1316, 2000, Kluwer Academic Publishers, The Netherlands, (2001), pp. 51–63.

[13] E. Boaknin, R. W. Hill, C. Proust, C. Lupien, L. Taillefer, and P. C. Canfield, Highly Anisotropic Gap Function in Borocarbide Superconductor $LuNi_2\ B_2C$, Phys. Rev. Lett. 87 (2001), pp. 237001-1–237001-4.

[14] A. Andreone, A. Cassinese, L. Gianni, M. Iavarone, F. Palomba, and R. Vaglio, Superconducting gap anisotropy of LuNi 2 B 2 C thin films from microwave surface impedance measurements, Phys. Rev. B 64 (2001), pp. 100505-1–100505-4(R).

[15] Zh.M. Tomilo, P.V. Molchan, A.S. Shestak, V.M. Finskaya, N.A. Prytkova, S.N. Ustinovich, Influence of annealing on the superconductivity of $ScNi_2\ B_2C$, Physica C, 361 (2001), pp. 95–98.

[16] K. Maki, P. Thalmeier, and H. Won, Anisotropic s-wave superconductivity in borocarbides $LuNi_2B_2C$ and $YNi_2\ B_2C$, Phys. Rev. B 65 (2002), pp. 140502-1–140502-4(R).

[17] Q. S. Yuan, and P. Thalmeier, BCS theory for s+g-wave superconductivity in borocarbides $Y(Lu)Ni_2B_2C$, Phys. Rev. B 68 (2003), pp. 174501-1–174501-5.

[18] P. Martinez-Samper, H. Suderow, S. Vieira, J. P. Brison, N. Luchier, P. Lejay, P. C. Canfield, Phonon-mediated anisotropic superconductivity in the Y and Lu nickel borocarbides, Phys. Rev. B 67 (2003), pp. 014526-1–014526-5.

[19] G. V. M. Kiruthika, G. Behr, R. Kulkarni, S.K. Dhar and L.C. Gupta, Y-induced stabilization of the superconducting phase in the $Sc1 - xY_xNi_2B_2C$ system, Physica C 405 (2004), pp. 245–252.

[20] D. R. Sanchez, E. M. Baggio-Saitovitch, H. Micklitz, and Sung-Ik Lee, Observation of a pair-breaking field in the magnetically diluted antiferromagnetic superconductor $DyNi_2B_2C$, Phys. Rev. B 71 (2005), pp. 024508-1–024508-5.

[21] C. L. Huang, J.-Y. Lin, C. P. Sun, T. K. Lee, J. D. Kim, E. M. Choi, S. I. Lee, and H. D. Yang, Comparative analysis of specific heat of YNi_2B_2C using nodal and two-gap models, Phys. Rev. B 73 (2006), pp. 012502-1–012502-4.

[22] J. Jensen and Per Hedegard, Competing magnetic and superconducting order in the rare-earth borocarbides RNi_2B_2C (R = Tm, Er, Ho, Dy), Phys. Rev. B 76 (2007), pp. 094504-1–094504-10.
[23] L. DeBeer-Schmitt, M. R. Eskildsen, M. Ichioka, K. Machida, N. Jenkins, C. D. Dewhurst, A. B. Abrahamsen, S. L. Budko, and P. C. Canfield, Pauli Paramagnetic Effects on Vortices in Superconducting $TmNi_2B_2C$, Phys. Rev. Lett. 99 (2007), pp. 167001-1–167001-4.
[24] M. Schneider, G. Fuchs, K.-H. Müller, K. Nenkov, G. Behr, D. Souptel, and S.-L. Drechsler, Magnetic pair breaking in superconducting $HoNi_2B_2C$ studied on a single crystal by thermal conductivity in magnetic fields, Phys. Rev. B 80 (2009), pp. 224522-1–224522-6.
[25] T. Baba, T. Yokoya, S. Tsuda, T. Watanabe, M. Nohara, H. Takagi, T. Oguchi, and S. Shin, Angle-resolved photoemission observation of the superconducting-gap minimum and its relation to the nesting vector in the phonon-mediated superconductor YNi_2B_2C, Phys. Rev. B 81 (2010), pp. 180509-1–180509-4(R).
[26] X. Lu, W. K. Park, S. Yeo, K.-H. Oh, S.-I. Lee, S. L. Budko, P. C. Canfield, and L. H. Greene, Superconducting order parameter in nonmagnetic borocarbides RNi_2B_2C (R = Y, Lu) probed by point-contact Andreev reflection spectroscopy Phys. Rev. B 83 (2011), pp. 104519-1–104519-10.
[27] F. Weber, L. Pintschovius, K. Hradil, and D. Petitgrand, Phonon line shapes in the vortex state of the phonon-mediated superconductor YNi_2B_2C, Phys. Rev. B 85 (2012), pp. 224525-1–224525-6.
[28] M. Weigand, L. Civale, F. J. Baca, Jeehoon Kim, S. L. Bud'ko, P. C. Canfield, and B. Maiorov, Strong enhancement of the critical current at the antiferromagnetic transition in $ErNi_2B_2C$ single crystals, Phys. Rev. B 87 (2013), pp. 140506-1–140506-5(R).
[29] F. Weber, L. Pintschovius, W. Reichardt, R. Heid, K.-P. Bohnen, A. Kreyssig, D. Reznik, and K. Hradil, Phonons and electron-phonon coupling in YNi_2B_2C, Phys. Rev. B 89 (2014), pp.104503-1–104503-13.
[30] D. Wulferding, I. Yang, J. Yang, M. Lee, H. Cheul Choi, S. L. Bud'ko, P. C. Canfield, H. W. Yeom, and J. Kim, Spatially resolved penetration depth measurements and vortex manipulation in the ferromagnetic superconductor $ErNi_2B_2C$, Phys. Rev. B 92 (2015), 014517-1–014517-6.
[31] L. F. Mattheiss, Electronic properties of superconducting $LuNi_2B_2C$ and related boride carbide phases, Phys. Rev. B 49 (1994), pp.13279–13282.
[32] L. F. Mattheiss, T. Siegrist, and R. J. Cava, Superconductivity in the $LnNi_2B_2C$ intermetallics via boron A_{1g} phonons, Solid State Commun. 91 (1994), pp.587–590.
[33] W. E. Pickett and D. J. Singh, $LuNi_2B_2C$: A novel Ni-based strong-coupling superconductor, Phys. Rev. Lett. 72 (1994), pp.3702–3705.
[34] P. Ravindran, S. Sankaralingam, and R. Asokamani, Electronic structure and phase-stability studies on superconducting YNi_2B_2C, YRh_3B, and nonsuperconducting YNi_4B Phys. Rev. B 52 (1995), pp. 12921–12930.
[35] J. I. Lee, T. S. Zhao, I. G. Kim, B. I. Min, and S. J. Youn, Electronic structure of Ni-based superconducting quaternary compounds:YNi_2B_2X (X= B, C, N, and Q), Phys. Rev. B 50 (1994),pp. 4030–4033.
[36] R. Coehoorn, Electronic structure of superconducting $LuNi_2B_2C$, YPd_2B_2C and related intermetallic compounds Physica C 228 (1994), pp.331–335.
[37] H. Kim, Chi-Duck Hwang, and J. Ihm, Ab initio pseudopotential calculations for the electronic structure of low-T_c $LuNi_2B_2C$ and the related compound LuNiBC, Phys. Rev. B 52 (1995), pp. 4592–4596.
[38] R. Weht, O.M. Cappannini, C.O. Rodrguez and N.E. Christensen, First-principles calculation of compressibilities and their pressure dependence in $LuNi_2B_2C$, Physica C, 260 (1996), pp. 125–129.
[39] O.M Cappannini, C.O Rodrguez, N.E Christensen, Pressure dependence of compressibilities in YNi_2B_2C and YPd_2B_2C, Physica C, 306 (1998), pp. 101–106.
[40] B.K Godwal, S Meenakshi, V Vijayakumar, R.S Rao and P Ravindran, High pressure studies on YNi_2B_2C and $LuNi_2B_2C$: ADXRD, Thermoelectric power, Resistivity, and Electronic structure, Journal of Physics and Chemistry of Solids, 59 (1998), pp. 2201–2204.
[41] K. Yamauchi, H. Katayama-Yoshida, A. Yanase and H. Harima, Band structure calculations and Fermi surfaces of YNi_2B_2C, Physica C, 412 (2004), pp. 225–229.
[42] K. Yamauchi and H. Harima, Bandstructure calculations and Fermi surfaces of RNi_2B_2C, Physica B 359–361 (2005) pp. 597–599.
[43] H. M. Tütüncü, H. Y. Uzunok, Ertuğrul Karaca, G. P. Srivastava, S. Özer, and Ş. Uğur, Ab initio investigation of BCS-type superconductivity in $LuNi_2B_2C$-type superconductors, Phys. Rev. B 92 (2015), pp.054510-1–054510-17.
[44] W. Reichardt, R. Heid, and K. P. Bohnen, Phonons and ElectronPhonon Coupling in Nickel Borocarbides, Journal of superconductivity 18 (2005), pp.759–761.
[45] P. Giannozzi, S. Baroni, N. Bonini, M. Calandra, R. Car, C. Cavazzoni, D. Ceresoli, G. L. Chiarotti, M. Cococcioni, I. Dabo, A.D. Corso, S. de Gironcoli, S. Fabris, G. Fratesi, R. Gebauer, U. Gerstmann, C. Gougoussis, A. Kokalj, M. Lazzeri, L. Martin-Samos, N. Marzari, F. Mauri, R. Mazzarello, S. Paolini, A. Pasquarello, L. Paulatto, C. Sbraccia, S. Scandolo, G. Sclauzero, A.P. Seitsonen, A. Smogunov, P. Umari and R.M. Wentzcovitch, QUANTUM ESPRESSO: a modular and open-source software project for quantum simulations of materials, J. Phys.: Condens. Matter 21 (2009), pp.395502-1–395502-19.
[46] D. Vanderbilt, Soft self-consistent pseudopotentials in a generalized eigenvalue formalism, Phys. Rev. B 41 (1990), pp.7892–7895.
[47] A. M. Rappe, K. M. Rabe, E. Kaxiras, and J. D. Joannopoulos, Optimized pseudopotentials, Phys. Rev. B 41 (1990), pp.1227–1230.
[48] J. P. Perdew, K. Burke, and M. Erzenrhof, Generalized Gradient Approximation Made Simple, Phys. Rev. Lett. 77 (1996), pp.3865–3868.
[49] W. Kohn and L. J. Sham, Self-Consistent Equations Including Exchange and Correlation Effects, Phys. Rev. 140 (1965), pp.A1133–A1138.
[50] H. J. Monkhorst and J. D. Pack, Special points for Brillonin-zone integrations, Phys. Rev. B 13 (1976), pp.5188–5192.
[51] A. Schmid, P. Pavone, and D. Strauch, Electron-phonon coupling in the metallic elements Al, Au, Na, and Nb: A first-principles study, Phys. Rev. B 57 (1998), pp.11276–11282.
[52] F. D. Murnaghan, The Compressibility of Media under Extreme Pressures, Proc. Nat. Acad. Sci. 30 (1944), pp.244–247.
[53] S. B. Dugdale, M. A. Alam, I. Wilkinson, R. J. Hughes, I. R. Fisher, P. C. Canfield, T. Jarlborg, and G. Santi, Nesting Properties and Anisotropy of the Fermi Surface of $LuNi_2B_2C$, Phys. Rev. Lett. 83 (1999) pp.4824–4827.
[54] P. B. Allen and R. C. Dynes, Transition temperature of strong-coupled superconductors reanalyzed, Phys. Rev. B 12 (1975), pp.905–922.
[55] P. Dervenagas, M. Bullock, J. Zarestky, P. Canfield, B. K. Cho, B. Harmon, A. I. Goldman, and C. Stassis,Soft phonons in superconducting $LuNi_2B_2C$, Phys. Rev. B 52 (1995) pp.R9839–R9842.
[56] Hyun-Jung Park, Hye-Soo Shin, Hye-Gyong Lee, In-Sang Yang, W. C. Lee, B. K. Cho, P. C. Canfield, and D. C. Johnston,Raman modes of RNi_2B_2C (R=Lu, Ho, Y) single crystals, Phys. Rev. B 53 (1996) 2237–2240.

Table 1. Lattice parameters (a and c), internal parameter (z), bulk modulus (B) and the pressure derivative of bulk modulus its pressure derivative ($B^{'}$) for $ScNi_2B_2C$ and their comparison with previous experimental and theoretical results. Selected interatomic separations (in $\mathring{A}$) and angles (α and β (in degrees) shown in Fig. 1) are also presented.

Source	$a(\mathring{A})$	$c(\mathring{A})$	z	d_{Ni-Ni}	$d_{B-C}(\mathring{A})$	$d_{Ni-B}(\mathring{A})$	α_{B-Ni-B}	β_{B-Ni-B}	B(GPa)	B
This work	3.39	10.62	0.3606	2.398	1.481	2.063	108.92^o	110.58^o	197.5	4
Experimental [3, 7]	3.34	10.21		2.362						
Experimental [15]	3.54	10.55		2.503						
Experimental [12]	3.34	10.68								
Experimental [19]	3.35	10.68								

Table 2. The zone-center phonon modes (ν in THz) and their electron-phonon coupling parameters (λ) for $ScNi_2B_2C$.

Mode	E_u	A_{2u}	B_{1g}	E_g	E_u	A_{2u}	E_u	E_g	A_{1g}	A_{2u}
ν	4.325	4.788	5.842	9.662	12.129	13.694	13.809	14.302	26.992	39.35
λ	0.014	0.018	0.078	0.0146	0.018	0.001	0.009	0.012	0.096	0.000

Table 3. Comparison of superconducting state parameters for $ScNi_2B_2C$ and $LuNi_2B_2C$. The parameter μ^* is taken to be 0.10 for both superconductors.

Perovskite	$N(E_F)$(States/eV)	ω_{ln}(K)	λ	T_C(K)
$ScNi_2B_2C$	3.33	265	0.93	16.28
$LuNi_2B_2C$ [43]	3.64	315	0.83	15.94

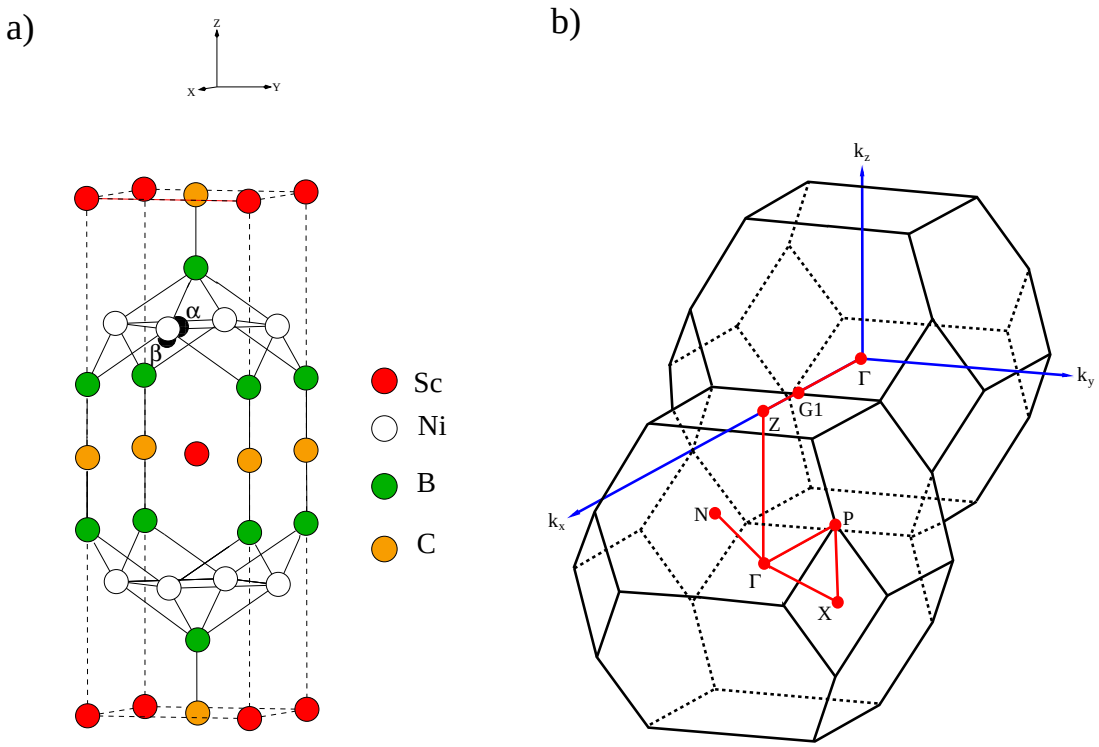

Figure 1. (a) The tetragonal unit-cell of $ScNi_2B_2C$. This structure basically contains NiB_4 tetrahedra between layers of ScC with rocksalt structure. (b) The Brillouin zone of body-centered tetragonal lattice. The high-symmetry points in the Brillouin zone in cartesian coordinates are: $\Gamma = \frac{2\pi}{a}(0.00,\ 0.00,\ 0.00)$, G1= $\frac{2\pi}{a}((\frac{1}{2}+\frac{a^2}{2c^2}),\ 0.00,\ 0.00)$, Z = $\frac{2\pi}{a}(1.00,0.00,0.0)$ or Z = $\frac{2\pi}{a}(0.00,0.00,\frac{a}{c})$, X= $\frac{2\pi}{a}(0.50,0.50,0.00)$, P= $\frac{2\pi}{a}(0.50,0.50,\frac{a}{2c})$, and N= $\frac{2\pi}{a}(0.0,0.50,\frac{a}{2c})$.Note that G1 is the zone boundary in the [100] direction. [Huseyin, I think that this BZ is for fcc lattice, but we need the BZ for bct (body centered tetragonal) lattice. What do you think?]

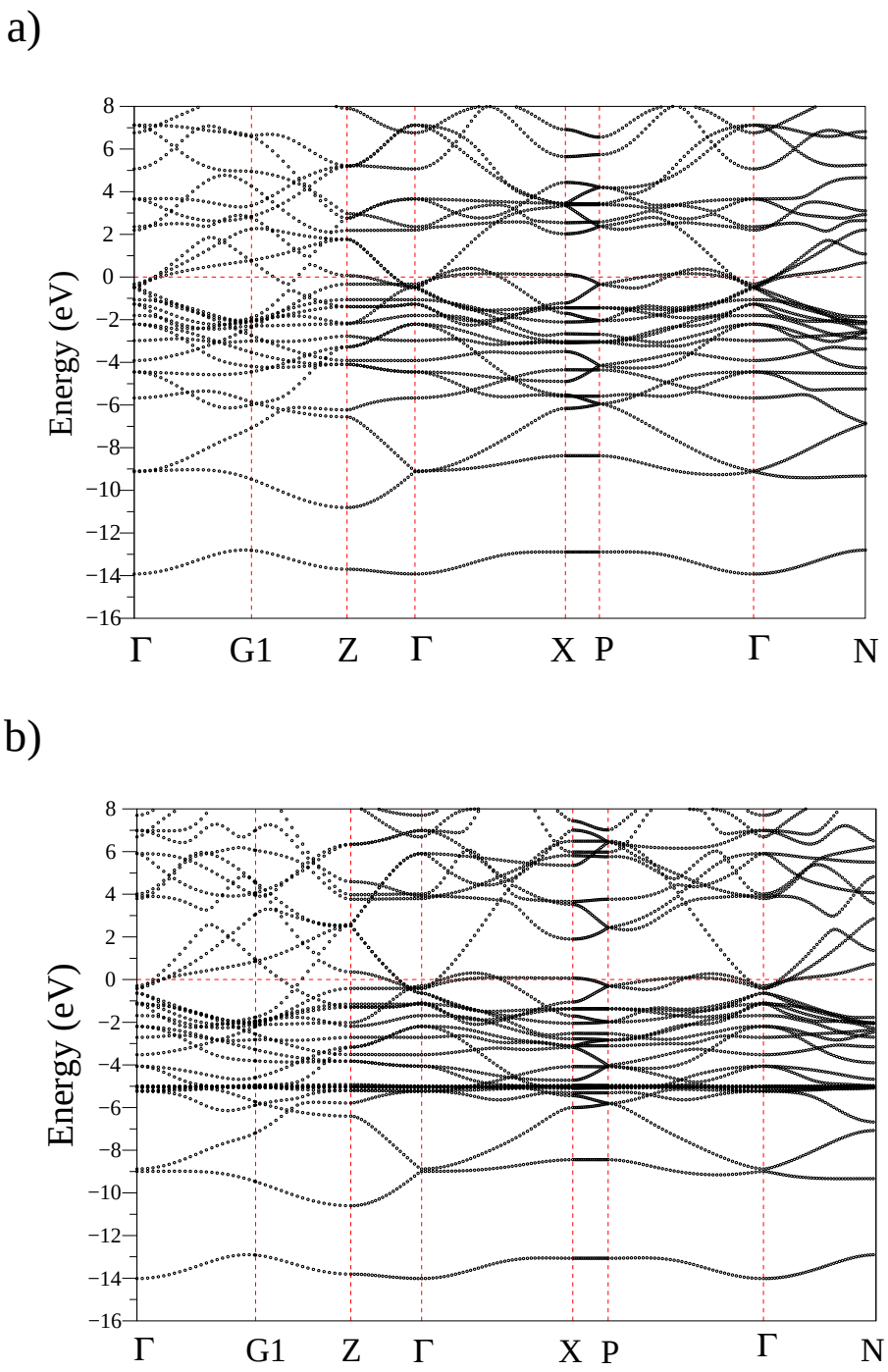

Figure 2. The electronic band structure for body-centered tetragonal $ScNi_2B_2C$ along several symmetry directions of the body-centered tetragonal Brillouin zone (see Fig. 1(b)). The Fermi level is fixed to 0 eV. (b) The electronic band structure of $LuNi_2B_2C$.

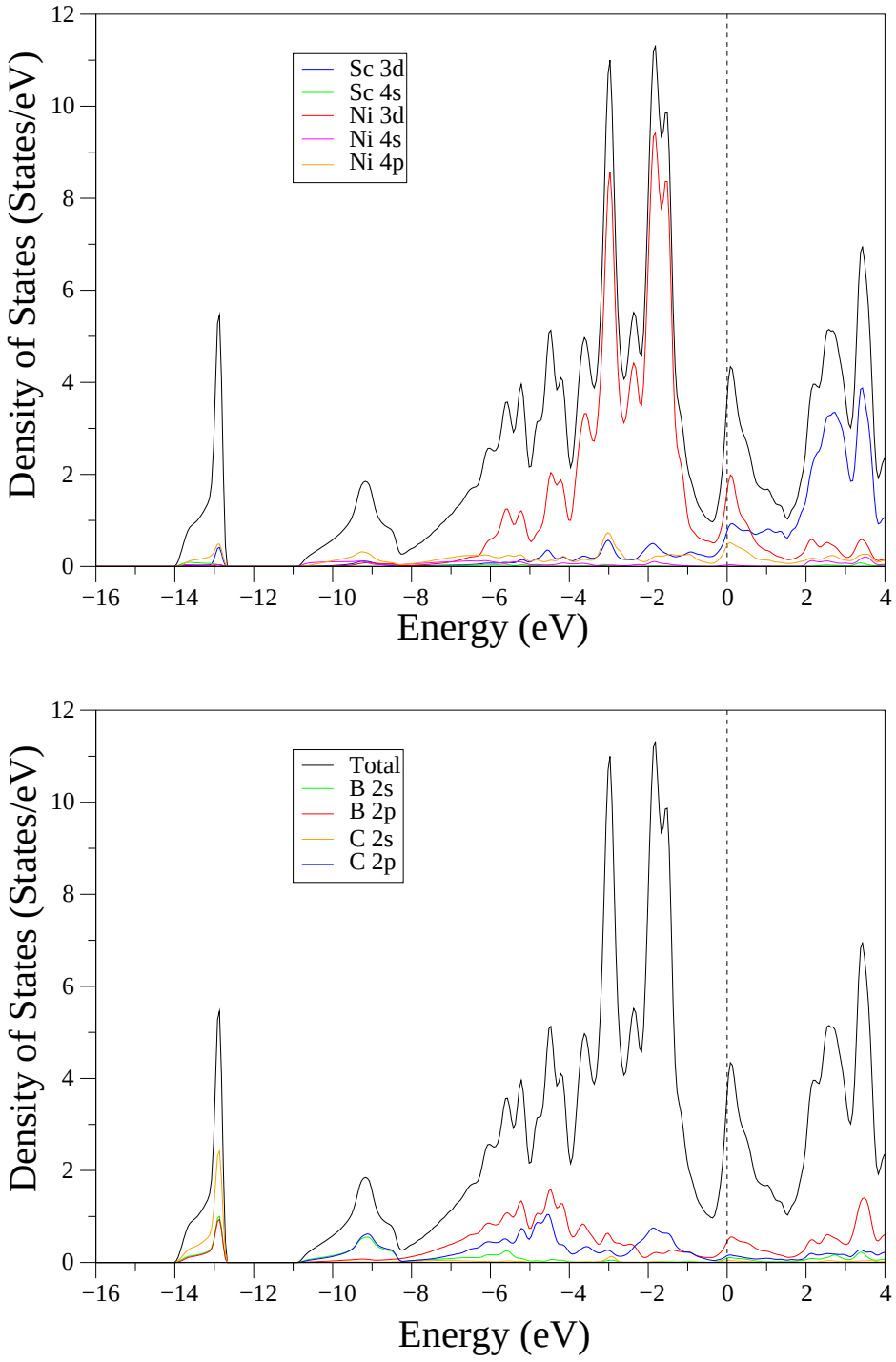

Figure 3. Total and partial electronic density of states for body-centered tetragonal $ScNi_2B_2C$.

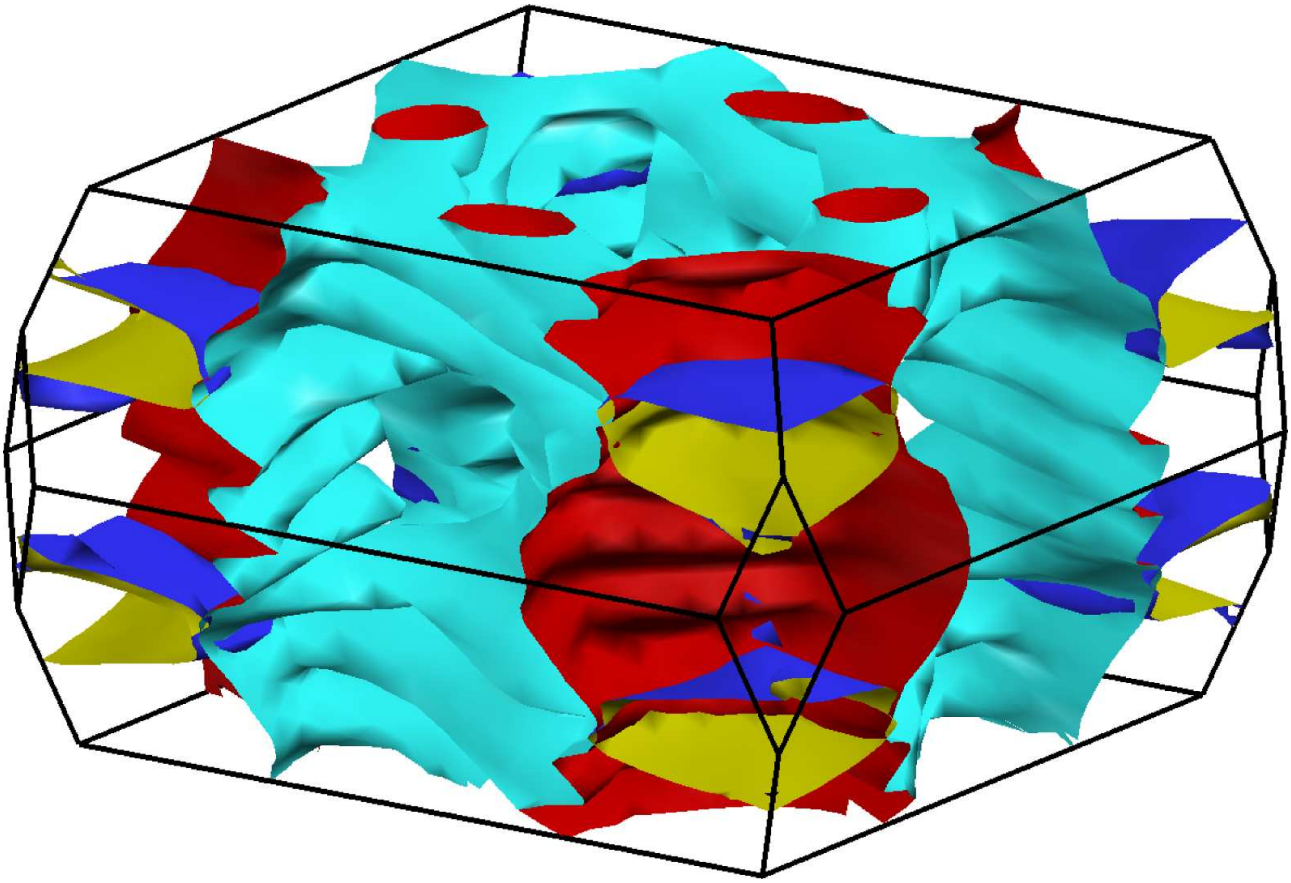

Figure 4. The calculated Fermi surfaces of $ScNi_2B_2C$. The characters of Fermi surfaces are primarily constituted by Ni 3d, Sc 3d, Ni 4d, and B and C 2p states.

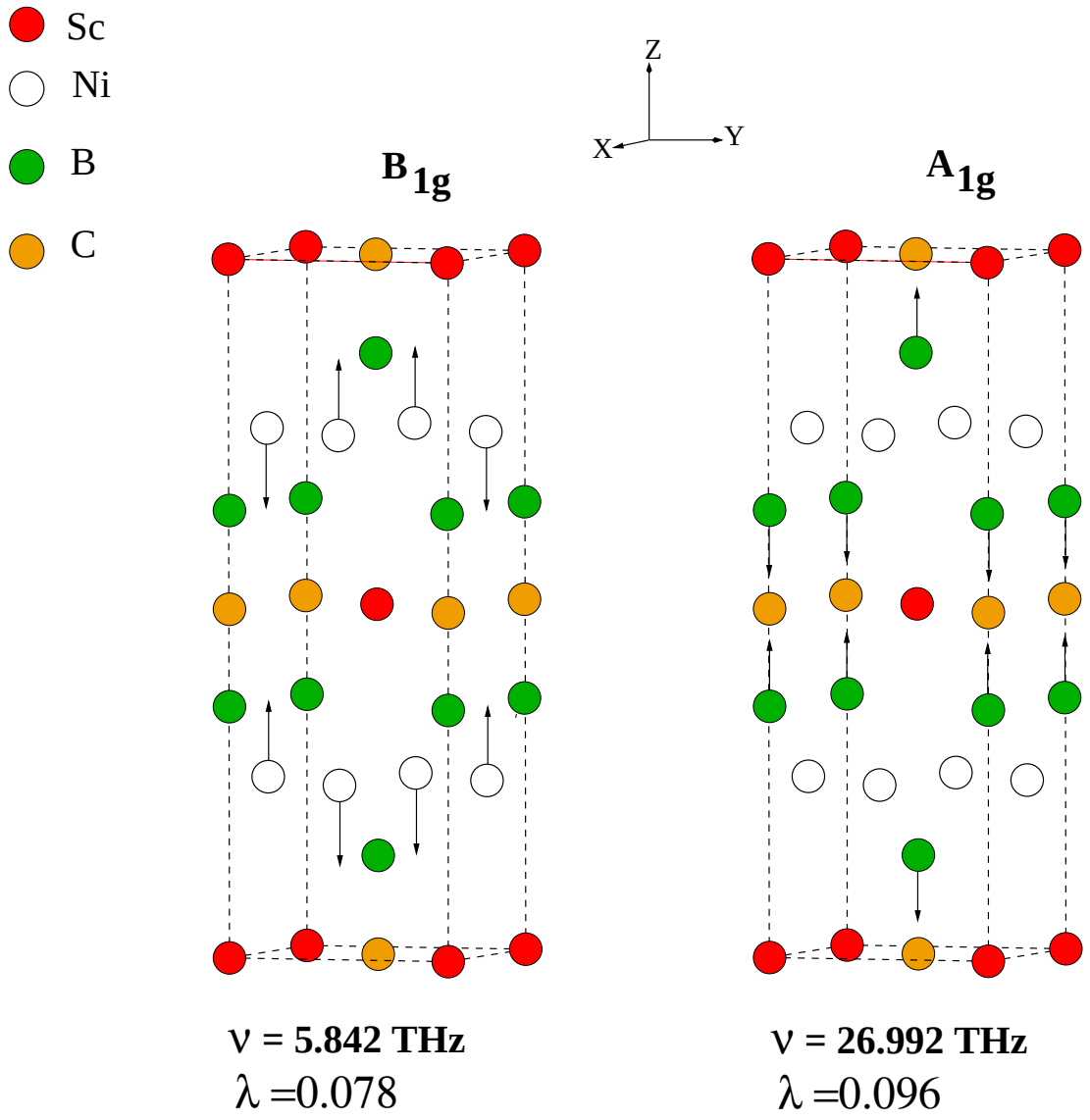

Figure 5. Eigenvector representations of the zone-centre B_{1g} and A_{1g} phonon modes in body-centered tetragonal $ScNi_2B_2C$.

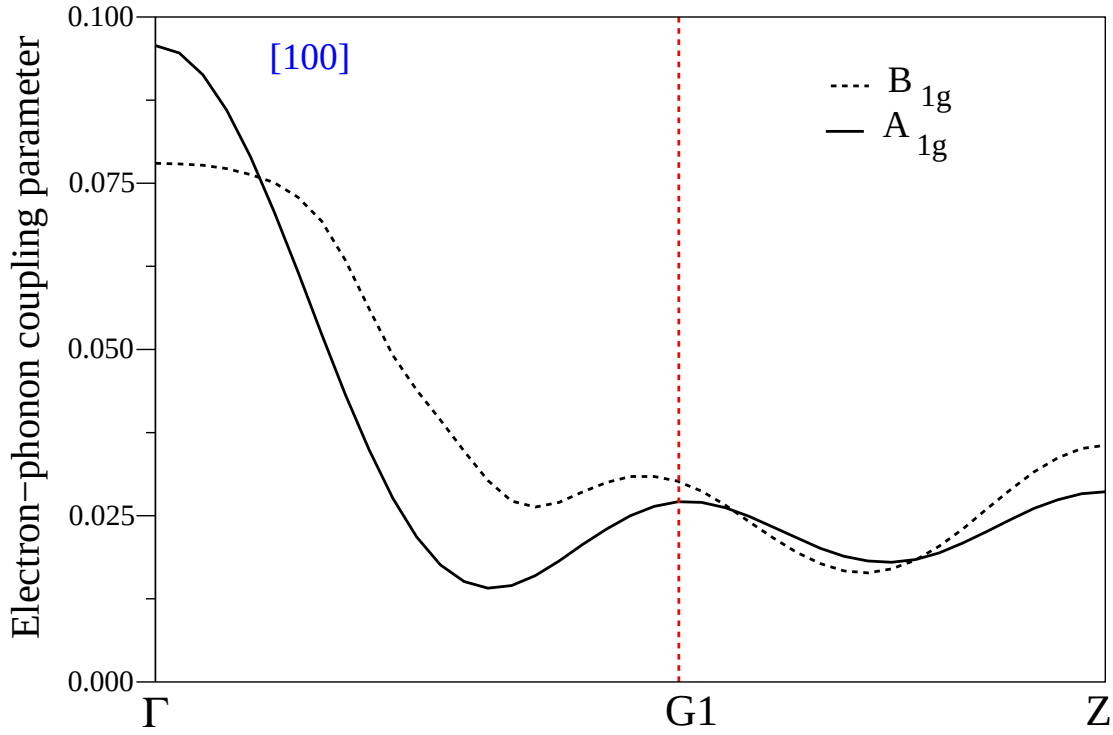

Figure 6. Calculated wavevector-dependent electron-phonon coupling parameter of the A_{1g} phonon mode for $ScNi_2B_2C$ along the [100] symmetry direction.

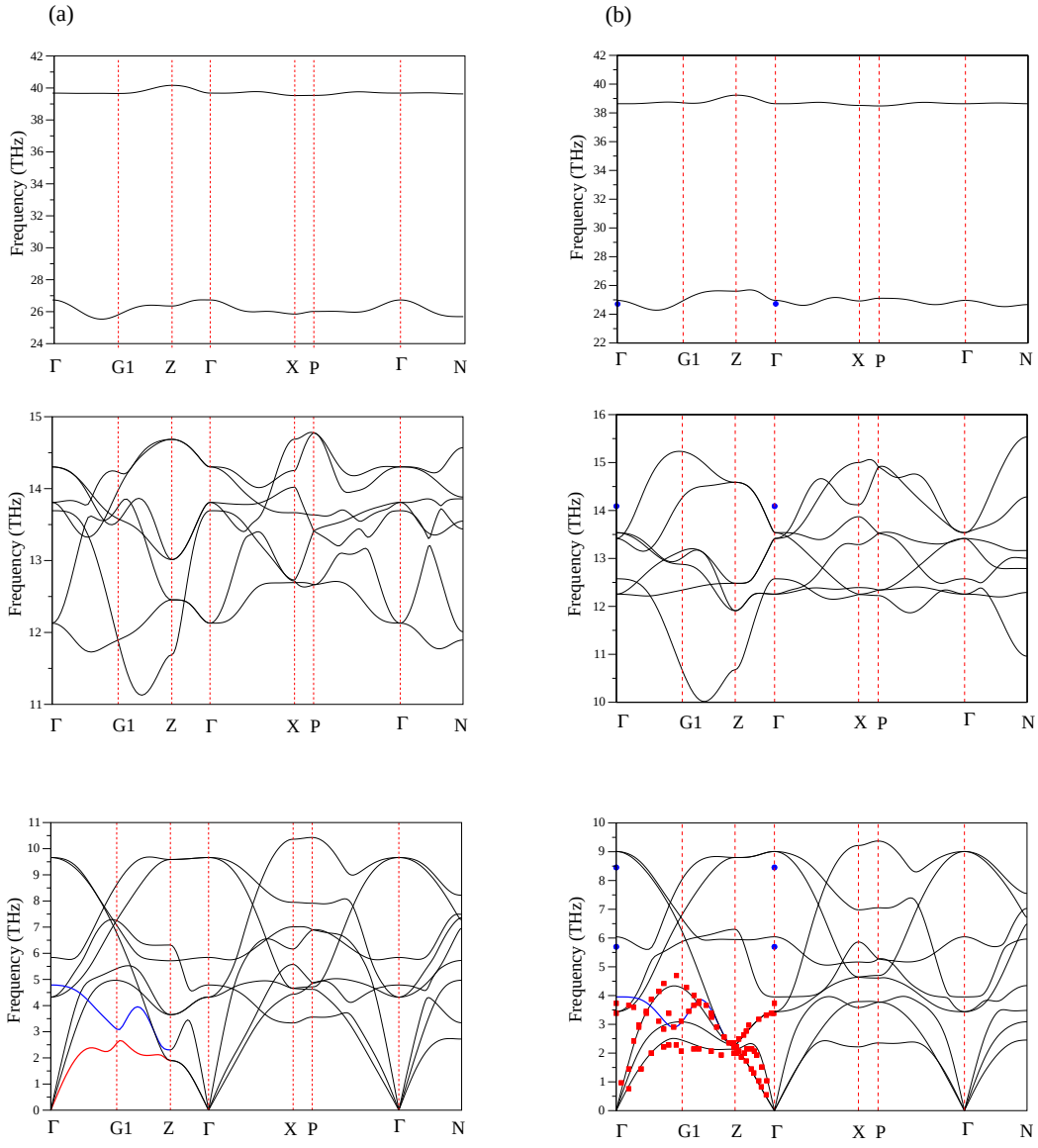

Figure 7. (a) Calculated phonon dispersion relations for body-centered tetragonal $ScNi_2B_2C$. The anomaly of the lower-lying transverse acoustic branch (TA_1) is shown by the red solid line and the anomaly of the A_{2u} branch is shown by the blue solid line. (b) Calculated phonon dispersion relations for body-centered tetragonal $LuNi_2B_2C$. Again the anomaly of the A_{2u} branch is shown by the blue solid line. In contrast to $ScNi_2B_2C$, the lowest transverse acoustic branch (TA_1) does not show any anomaly. Inelastic-neutron-scattering results [55] and Raman results are shown by red squares and blue circles [56], respectively.

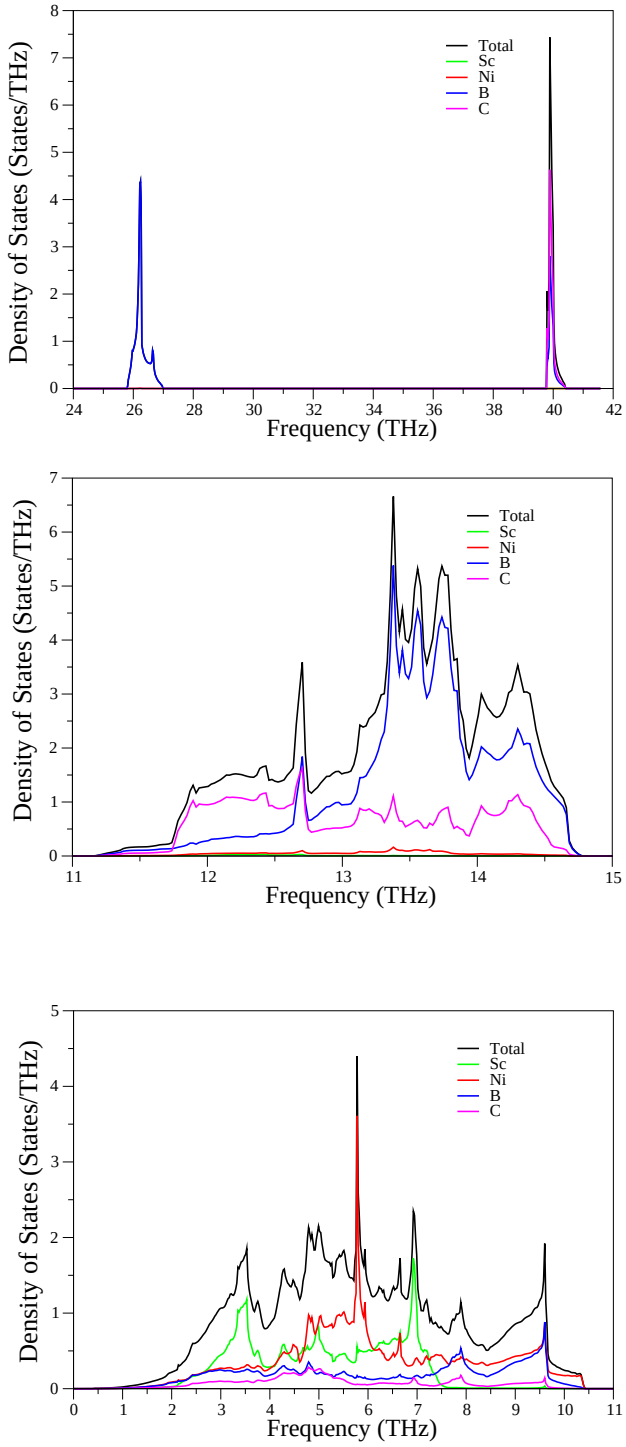

Figure 8. The calculated phonon total and atom-projected density of states for the body centered tetragonal $ScNi_2B_2C$.

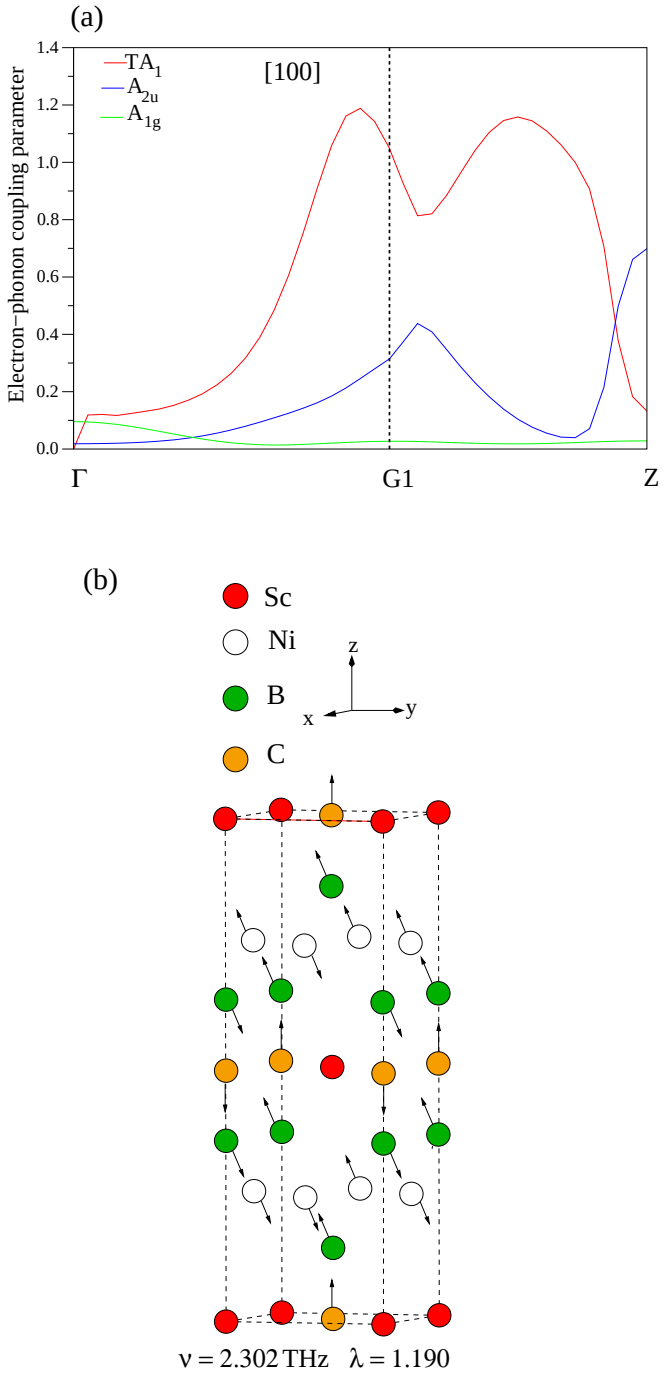

Figure 9. (a) Calculated wavevector dependent electron-phonon coupling paremeter for the lower transverse acoustic branch (TA_1) and the A_{2u} branch. For comparison, the wavevector dependent electron-phonon coupling paremeter for the A_{1g} branch is also shown. (b) The eigenvector representation of the lower transverse acoustic phonon branch (TA_1) at $\boldsymbol{q} = \frac{2\pi}{a}$ (0.5, 0.0, 0.0).

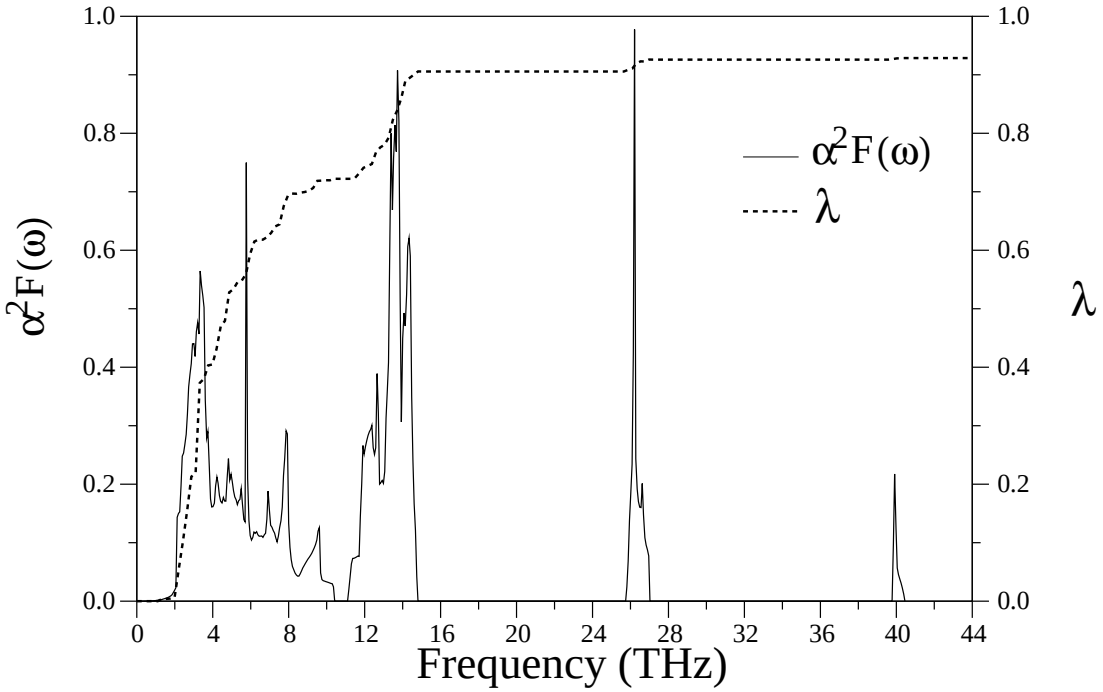

Figure 10. Calculated electron-phonon spectral function $\alpha^2F(\omega)$ (solid line) and the frequency-accumulated electron-phonon coupling parameter λ (dashed line) for $ScNi_2B_2C$.